Imaging of *Caenorhabditis elegans* neurons by second-harmonic generation and two-photon excitation fluorescence

George Filippidis
Christos Kouloumentas
Foundation of Research and Technology-Hellas
Institute of Electronic Structure and Laser
P.O. Box 1527
Heraklion, Greece 71110
E-mail: filip@iesl.forth.gr

Giannis Voglis
Foundation of Research and Technology-Hellas
Institute of Molecular Biology and Biotechnology
Vassilika Vouton
Heraklion, Greece 71110

Fotini Zacharopoulou
Theodore G. Papazoglou
Foundation of Research and Technology-Hellas
Institute of Electronic Structure and Laser
P.O. Box 1527
Heraklion, Greece 71110

Nektarios Tavernarakis
Foundation of Research and Technology-Hellas
Institute of Molecular Biology and Biotechnology
Vassilika Vouton
Heraklion, Greece 71110

Abstract. Second-harmonic generation (SHG) and two-photon excitation fluorescence (TPEF) are relatively new and promising tools for the detailed imaging of biological samples and processes at the microscopic level. By exploiting these nonlinear phenomena phototoxicity and photobleaching effects on the specimens are reduced dramatically. The main target of this work was the development of a compact inexpensive and reliable experimental apparatus for nonlinear microscopy measurements. Femtosecond laser pulses were utilized for excitation. We achieved high-resolution imaging and mapping of *Caenorhabditis elegans* (*C. elegans*) neurons and muscular structures of the pharynx, at the microscopic level by performing SHG and TPEF measurements. By detecting nonlinear phenomena such as SHG and TPEF it is feasible to extract valuable information concerning the structure and the function of nematode neurons. © *2005 Society of Photo-Optical Instrumentation Engineers.* [DOI: 10.1117/1.1886729]

1 Introduction

Nonlinear phenomena have proven to be powerful tools in biological imaging. Molecular excitation by the absorption of two or more photons can be advantageous for specific imaging applications over standard fluorescence microscopy, which is based on the absorption of a single photon. Such applications are the two-photon[1] and three-photon[2] excitation fluorescence microscopy (TPEF and 3PEF respectively), or more generally, multiphoton excitation fluorescence microscopy.[3] Second-harmonic generation (SHG) has also emerged as a powerful contrast mechanism in nonlinear microscopy. It has been demonstrated that its combination with TPEF in a single microscope can be very advantageous, since they provide complementary information about several biological processes.[4,5] The information provided by the two contrast techniques can be differentiated based on the fundamentally different phenomena underlying TPEF and SHG.[6] While TPEF relies on nonlinear absorption of the incident light and fluorescence emission, SHG relies on nonlinear scattering and does not involve an excited state, hence the first is not a coherent process, whereas the second one is. In SHG, light of the fundamental frequency ω is converted by nonlinear materials into light at exactly twice that frequency, 2ω. An indicated and reliable solution for the collection and the wave-length separation of the low-intensity signals (SHG and TPEF) is the combination of lock-in detection with a monochromator. This configuration was followed for the detection of our signals, while other detection schemes, such as single photon counting, are also feasible in collecting very weak signals.

Both TPEF and SHG exhibit intrinsic three-dimensionality and ability to section deep within biological tissues, due to their nonlinear nature. They both have significant efficiency only at extremely high incident light intensities, and therefore arise only from a well-defined volume around the focal center of the incident light beam. In both TPEF and SHG, the wavelength of the fundamental incident light lies in the infrared (IR) spectrum region, thus suffering less scattering and absorption inside the biological samples and exhibiting larger penetration depths. SHG and TPEF microscopy methodologies do not exhibit higher resolution compared to confocal one-photon microscopy.[7] However, as far as the axial direction is concerned, the excitation of the biological specimen in SHG and TPEF microscopy is confined in a small region around the focal plane, due to the quadratic dependence of SHG and TPEF intensities upon the excitation photon flux. "Out-of-focal-plane" photobleaching and phototoxicity are thus dramatically reduced, permitting higher possibilities of survival in the biological specimen during *in vivo* experiments.

Address all correspondence to George Filippidis, IESL, FORTH, Vassilika Vouton, Heraklion, Crete 71110 Greece; Tel: ++30 2810 391323; Fax: ++30 2810 391318; E-mail: filip@iesl.forth.gr

Since SHG does not come from an absorptive process, photodamage does not arise intrinsically during SHG microscopy. However, if the incident beam produces simultaneously two-photon excitation of chromophores in the sample, photobleaching also accompanies SHG. This happens when the energy of the second-harmonic signal overlaps with an electronic absorption band.[8] This is usually the case when the magnitude of the SHG signal is resonantly enhanced. Because SHG is a coherent phenomenon, the produced second-harmonic signal is highly directional and propagates forward in the direction of the fundamental collimated beam, forming a single lobe. However, when the incident beam is tightly focused, the SHG radiation pattern exhibits two separate lobes.[9] Mertz and colleagues theoretically described the case of SHG from an inhomogeneous sample by highly focused excitation light and concluded that these inhomogeneities can significantly modify the SHG radiation patterns, and in some cases, can provoke backward SHG propagation.[10–13]

Molecular frequency doubling is caused by the nonlinear dependence of the induced dipolar moment μ of the molecule on the incident optical electric field E. Thus μ can be expanded in a Taylor's series about $E = 0$:

$$\mu = \mu_o + \alpha * E + \frac{1}{2} \beta * E * E + \frac{1}{6} \gamma * E * E * E + \ldots \quad (1)$$

where μ_o is the permanent dipolar moment of the molecule, α is the linear polarizability, β is the molecular first hyperpolarizability, which governs in the molecular level SHG, and γ is the second hyperpolarizability which governs among others multiphoton absorption and 3HG.[6,14] Macroscopically the optical response of materials to incident light, or generally electromagnetic radiation, is characterized by the optically induced polarization density, P, which can also be expanded in a Taylor's series about $E = 0$:

$$P = \chi^{(1)} * E + \chi^{(2)} * E * E + \chi^{(3)} * E * E * E + \ldots \quad (2)$$

where P represents the polarization density vector, and $\chi^{(n)}$ are the nth order optical susceptibility tensors. The first term describes linear absorption and reflection of light, the second term describes SHG, sum, and difference frequency generation, and the third term covers multiphoton absorption, third-harmonic generation, and stimulated Raman processes. The macroscopic second order susceptibility tensor $\chi^{(2)}$, which is responsible for SHG, is related to the molecular first hyperpolarizability, β, by:

$$\chi^{(2)} = N \langle \beta \rangle \quad (3)$$

where N is the spatial density of molecules, and $\langle \beta \rangle$ represents an orientational average.[15] Equation (3) implies that only non-centrosymmetric materials have a nonvanishing second order susceptibility $\chi^{(2)}$, and the coherent summation of their single molecules' SHG radiation patterns are not cancelled out, resulting in a highly directional, detectable second-harmonic signal. The second-harmonic intensity in such media scale as:[15]

$$SHG_{sig} \propto p^2 \tau (\chi^{(2)})^2 \quad (4)$$

where p and τ are the laser pulse energy and pulse width, respectively. Combining Eqs. (3) and (4), it is apparent that the second-harmonic intensity is proportional to N^2, whereas TPEF intensity is known to be proportional to N. The quadratic dependence of the second-harmonic intensity on the spatial density of molecules is somewhat expected, since the single molecules act as dipole radiators and the total SHG signal arises from their constructive interference. By contrast the TPEF is a noncoherent phenomenon, and the radiation of each fluorescent molecule is independent from the emission of the neighboring molecules.

Under the symmetry constraints it is obvious that SHG can mainly be produced at interfaces, where the symmetry breaks, from metal surfaces, where there is a huge change in the refractive indices, and from structures that have a high degree of orientation and organization but lack inversion symmetry, such as specific crystals. Dyes bounded in cellular membranes and endogenous arrays of structural proteins can also produce SHG, which is of significant biological interest.

In 1962, Kleinmann first demonstrated SHG in crystalline quartz[16] and in 1974, Hellwarth first integrated SHG into an optical microscope to visualize the microscopic crystal structure in polycrystalline ZnSe.[17] Freund and colleagues performed one of the first biological SHG imaging experiments in 1986,[18] in a successful effort to study the endogenous collagen structure in a rat tail tendon at approximately 50 μm resolution. Over the last few years many efforts have been successful in three-dimensional SHG imaging of endogenous structural proteins,[5,15,19–25] without the addition of fluorescent dyes, as in the case of TPEF microscopy.[4] Structural proteins that form highly ordered, birefringent arrays such as collagen, actomyosin complexes, and tubulin, from many animal sources (tetra fish, the nematode worm *C. elegans*, mouse, and chicken), produce relatively strong SHG signals. Collagen especially, which has a highly crystalline not centrosymmetric triple-helix structure, produces SHG extremely effectively.[26,27]

One of the innovative applications of SHG is its usage as a highly sensitive monitor of membrane potential.[28–35] When laser pulses are incident on a membrane they induce membrane bound dipoles making them candidates for SHG. The observed SHG signal originates only from the asymmetrically distributed dipoles of the membrane.[36] Alterations in the membrane potential alter the magnitude of the induced dipoles, thus affecting the magnitude of the observed SHG signal. Green fluorescent protein (GFP) has been used as a SHG probe in this way[32,37] because it undergoes large electron redistribution in the presence of light, and the resulted induced dipole is affected by the characteristics of the transmembrane potential. Khatchatouriants and colleagues used GFP as an SHG probe to monitor alterations of membrane potential in *C. elegans* neurons.[37]

Caenorhabditis elegans is a small (1-mm) free-living hermaphroditic nematode that completes a life cycle in 2.5 days at 25 °C. The simple body plan and transparent nature of both the egg and the cuticle of this nematode have facilitated an exceptionally detailed developmental characterization of the animal. The complete sequence of cell divisions and the normal pattern of programmed cell deaths that occur as the fertilized egg develops into the 959-celled adult are known.[38] One considerable advantage of the *C. elegans* system is that it

is the first metazoan for which the genome was sequenced to completion.[39] Investigators can take advantage of genome data to perform "reverse genetics," directly knocking out genes. Mutations can be easily induced and large screens can be performed to isolate mutants having specific phenotypes. In addition, a novel method of generating mutant pheno-copies, called doublestranded RNA-mediated interference (RNAi), enables probable loss-of-function phenotypes to be rapidly evaluated.[40] Another advantage of this system is that construction of transgenic animals is rapid; DNA injected into the hermaphrodite gonad concatamerizes and is packaged into embryos, hundreds of which can be obtained within a few days of the injection.[41] The anatomical characterization and understanding of neuronal connectivity in *C. elegans* are un-paralleled in the metazoan world. Serial section electron microscopy has identified the pattern of synaptic connections made by each of the 302 neurons of the animal (including 5000 chemical synapses, 600 gap junctions, and 2000 neuro-muscular junctions), so that the full "wiring diagram" of the animal is known.[42] Although the overall number of neurons is small, 118 different neuronal classes, including many neu-ronal types present in mammals, can be distinguished. Other animal model systems contain many more neurons of each class (there are about 10,000 more neurons in *Drosophila* with approximately the same repertoire of neuronal types). Overall, the broad range of genetic and molecular techniques applicable in the *C. elegans* model system allows a unique line of investigation into fundamental problems in biology.

The coordinated function of individual *C. elegans* neurons leads to characteristic behavioral responses. Although system-atic investigations have revealed important information about the neurons that participate in specific behaviors,[43–45] the mo-lecular and physiological processes underlying neuronal func-tion remain poorly understood.

A low cost, flexible, reliable system was developed for the nonlinear imaging of the samples in this study. We present a detailed mapping of the nematode *C. elegans* in its anterior and posterior body parts using TPEF and SHG scanning im-ages. Mutants, which express GFP in the pharyngeal muscle cells, have been imaged using both phenomena. Additionally, animals that express GFP in the cytoplasm of the six mecha-noreceptor neurons, as well as animals expressing GFP bound to the membrane of these cells, have been investigated. We focused our research on the posterior part of the nematode, where two of these six neurons are located, and we ascer-tained that the SHG signal level, arising from the structural protein arrays, is also very significant in this region of the worm.

2 Experimental Apparatus

We used a femtosecond t-pulse laser (high power femtosec-ond oscillator from Amplitude Systems) as an excitation source, in our experiments. This source is a compact diode-pumped femtosecond laser oscillator, which delivers a train of high energy, short duration pulses. The laser material is an ytterbium doped crystal. Ytterbium belongs to the rare earths family, and has strong absorption bands in the near-infrared (940–980 nm depending on the host matrix). The small size of the laser permits the whole setup to be extremely flexible. The average power of the laser was 1 W, the pulse duration

less than 200 fs and the repetition rate 50 MHz. The laser emission wavelength was at 1028 nm in order to maintain a high efficiency on the excitation of GFP molecules. The beam was directed to a modified optical microscope (Nikon Eclipse ME600D) using a suitable pair of mirrors and was focused tightly onto the sample by an objective lens of high numerical aperture (Nikon 50X N.A. 0.8). The average laser power on the specimen was 10 mW. A CCD camera (Sony XC-57CE) was used for observation of the sample through the objective and suitable optics. Both an ultrafast laser and tight focusing are necessary for the realization of the high intensities re-quired for nonlinear phenomena such as SHG and TPEF. Bio-logical samples were placed on standard coverslips that fit into a motorized xyz translation stage (Standa 8MT167-100). The minimum step of the stages in each direction is 1 μm. The choice of a motorized stage represents an inexpensive and reliable solution for the realization of the scanning proce-dure. Its main advantage is the low cost in comparison with expensive commercial galvano-mirrors. It is feasible to per-form reliable and precise imaging of biological samples and *in vivo* measurements in real time by using this inexpensive scanning configuration.

TPEF signals were collected using a photomultiplier tube (PMT Hamamatsu R4220) connected to a lock-in amplifier (SR810 Stanford Research Systems). The photomultiplier tube was attached at the position of the eyepiece of the mi-croscope. A short pass filter (SPF 650 nm CVI) was placed at the photomultiplier input in order to cut off the reflected laser light. By using the Labview program (National Instruments, Labview 6.1), which was developed specifically for this ap-plication, we were able to control the movement of the step motors and to record the signals in every step during the scan-ning procedure. The average accumulation time in every step was 30 ms.

Since SHG is a coherent process, most of the signal is transmitted towards the direction of the fundamental beam. For thin samples (such as *C. elegans*) almost the entire signal propagates with the laser and was collected and collimated by the condenser lens (Nikon N.A. 0.9). The condenser lens was properly aligned below the xyz motorized stage. The numeri-cal aperture of the condenser lens must be equal or higher when compared to the objective lens in order to collect the whole cone of light. A dichroic mirror (99% at 45 deg, 450–550 nm) was used to reflect the transmitted beam. A mono-chromator (Digikrom CM110 CVI) was employed in order to distinguish the SH from the two-photon fluorescence signal and to provide spectral information. The resolution of the monochromator was 1 nm. This resolution (1 nm) was neces-sary since we want to achieve the best separation between SHG and TPEF signals in the forward detection scheme. The detected signals in the forward direction were in sufficiently high intensities, despite the very thin spectral range under investigation. A filter (SPF 700 nm CVI) was used in front of the monochromator to cut off the residual fundamental laser light. By using this configuration we were able to record SHG and TPEF signals in distinct sets of measurements by tuning the monochromator in different spectral regions. For the de-tection of the signals a photomultiplier tube (PMT Hamamatsu R636-10) connected to the lock-in amplifier was used. The resolution of our experimental setup is 1 μm, lim-
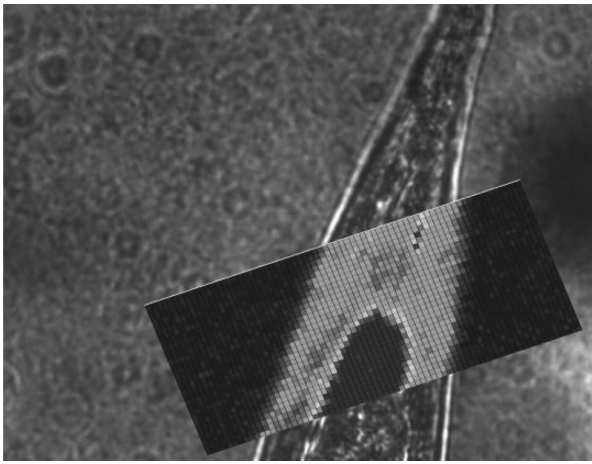
Fig. 1 Two-photon excitation fluorescence image from the posterior part of a *C. elegans.*

ited by the beam waist of the objective lens and the minimum step of the xyz translation stage.

3 Sample Preparation

3.1 *Nematode Strains and Growth*

We followed standard procedures for *C. elegans* strain maintenance, crosses and other genetic manipulations.[46] Nematode rearing temperature was kept at 20 °C. Before each experiment, young adult animals were anaesthetized by immersing to 0.5 M of sodium azide (NaN$_3$), and were subsequently mounted on glass slides.

4 Results

The target of this study is the development of an inexpensive, compact, and reliable experimental apparatus for the detailed imaging and mapping of *C. elegans* neurons and other structural components, by performing second-harmonic generation (SHG) and two-photon excitation fluorescence (TPEF) measurements. The use of an infrared wavelength (1028 nm) as an excitation source provides negligible photobleaching and phototoxication to the sample due to the low energy per photon. The nonlinear nature of the recorded phenomena insures that the effect will be confined only to the focal region, thus dramatically improving the spatial resolution by minimizing out-of-focus phenomena such as fluorescence. So, there is no need to perform confocal microscopy measurements when nonlinear phenomena such as SHG and TPEF are detected.

Figure 1 depicts the TPEF image from the posterior end of *C. elegans.* The signal was captured from above. In this transgenic line, GFP is expressed under the control of the *mec*-4 promoter in the six mechanoreceptor neurons of the animal. For the realization of the measurements, due to the limited quantity of GFP molecules onto the sample, an objective lens with high numerical aperture (100X NA 1.25 oil immersion) was employed for tight focusing. In Fig. 1 the contour of the worm, the region of intestine, and a neuronal cell can be clearly seen. The dimensions of the scanning region were 30×70 μm^2. Two of the six mechanoreceptor neurons are located in the posterior part (tail) of the worm usually in dif-

ferent z positions. The scanning was performed in a specific z position where the TPEF signal arising from one neuron was maximum.

The autofluorescence intensity in the tail of *C. elegans* is weaker than the TPEF from GFP molecules except from the region of the gut. The neurons we are imaging in the tail of *C. elegans* (PLML—PLMR) do not overlap with the gut and are situated more posteriorly. Their somata are situated close to the tip of the tail away from the gut autofluorescence. The dimensions of the body and the neuronal axon of a *C. elegans* mechanoreceptor neuron are 2 μm and 200 nm respectively. The dimensions of the region where the TPEF signal from GFP molecules were recorded are similar (Fig. 1). The limitation to the spatial resolution of our setup due to the minimum step of the scanning stage (1 μm) must also be taken into account. The high intensity of the signal, the position, and the dimensions of this region in the tail of the worm, as well as the reproducibility of the images which were obtained by performing TPEF imaging to similar specimens, lead us to the conclusion that the recorded signals came from the GFP molecules which are expressed in fusion with the MEC-4 protein in the mechanoreceptor neuron of the worm.

Endogenous structural proteins of the worm, such as collagen, are responsible for the detection of the weak autofluorescence signal arising from the contour of *C. elegans*. On the other hand, the main contribution in the high signal, which were recorded from the intestine, comes from the lipid inclusions. Thus, by performing TPEF imaging measurements in *C. elegans*, unique and reliable information can be extracted about the structure and the morphology of specific cell types in the worm.

Figure 2 depicts the spectral distribution of the recorded signal from the pharynx of the worm. GFP is expressed in the pharyngeal muscle cells of *C. elegans*. The signal was collected from below. There is a main peak at 514 nm, which abruptly reduces as the monochromator setting was changed by 5–6 nm around this wavelength. This observation is in perfect agreement with the spectral distribution, which presents the nonlinear phenomenon of second-harmonic generation. Furthermore, the signal appears at the expected spectral bandwidth of ∼4 nm full width at half maximum (the laser fundamental has a FWHM of ∼6 nm). For a Gaussian profile, the bandwidth of the SHG signal scales as a square root $(1/\sqrt{2})$ of the fundamental bandwidth. The inset of Fig. 2 shows the magnification of the same spectral distribution. The collected signal exclusively comes from TPEF for $\lambda > 518$ nm. As was expected, the spectrum of two-photon excitation fluorescence does not present any abrupt reduction over a few nanometers. Due to the excitation wavelength (1028 nm), the signal at 514 nm comprises both SHG and TPEF. The independently measured SHG signal is at least 30 times stronger than the TPEF counterpart. Consequently, the dominant contribution at 514 nm comes from SHG signals.

Figure 3(a) represents a TPEF image of the anterior part of *C. elegans*. The signal was recorded from below. The monochromator was tuned at 525 nm, so the detection of the signal was performed in a spectral region where the contribution of SHG had been excluded. The GFP molecules are expressed in the cytoplasm of the pharyngeal muscle cells of the worm. The dimensions of the scanning region were 34×66 μm^2. The scanning was obtained in a specific z position where the col-
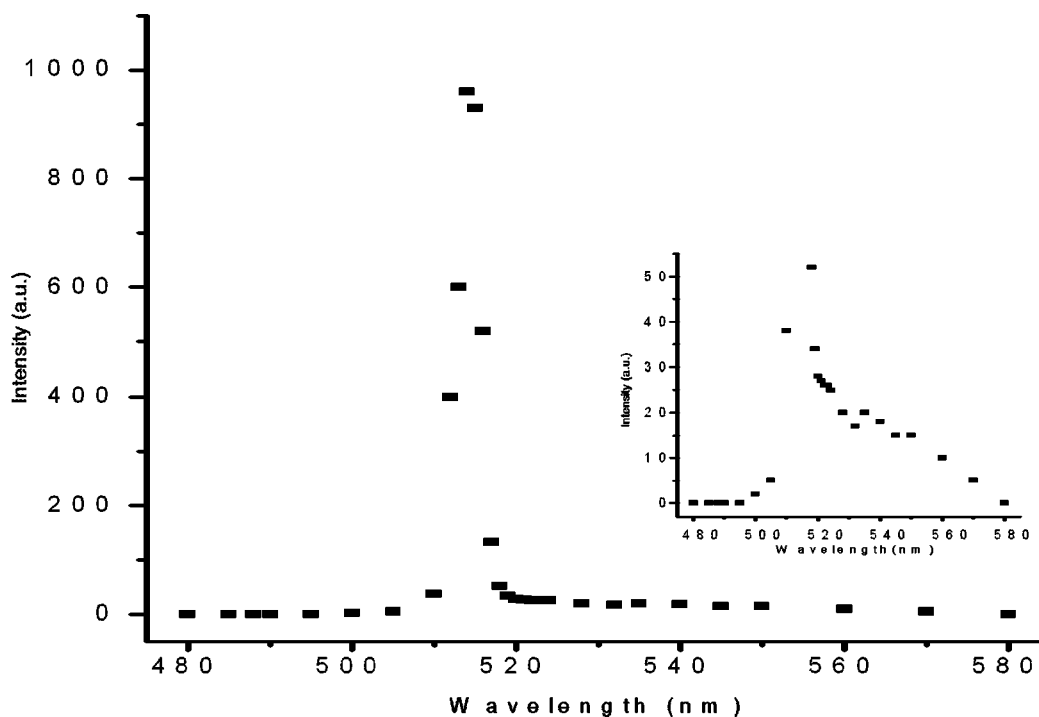
Fig. 2 Spectral distribution of the collected signal from a pharynx of a *C. elegans.*

lected TPEF signal that comes from the pharynx became maximum. The signal from TPEF originated from the inner part of the pharynx, where the GFP molecules were located. The shape and the morphology of the pharynx of the worm can be observed with satisfactory resolution.

Figure 3(b) shows the same scanning of *C. elegans* but in this case the monochromator was tuned at 514 nm. Therefore, the SHG is the dominant factor in the collected signals. As already mentioned in the introduction, structures of well-ordered protein assemblies, such as collagen and actomyosin complexes, are efficient SHG sources. We hypothesize that

these endogenous structural protein arrays are the main contributors to the recorded signals based on other studies.[5,15,19] In addition, the SHG image [Fig. 3(b)] shows clearly the body wall muscles and the pharyngeal muscles, indicating that the detected SHG signal originates mainly from actomyosin complexes and collagen. In Fig. 3(b) the structures of high SHG intensity in the middle of the body appear to have a thickness of 3–4 μm, which corresponds to the real thickness of the pharyngeal muscles of the worm. This is an indication that the actomyosin complexes, which mainly form the sarcomeres, are the main contributors to the SHG recorded signals from
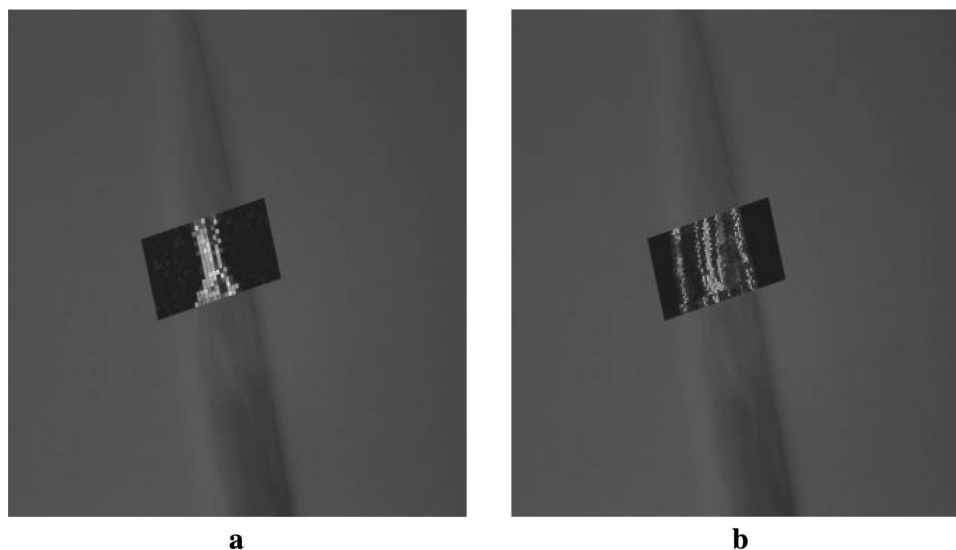

Fig. 3 Two-photon excitation fluorescence image (a) and second-harmonic generation image (b) respectively. Images were recorded from the forward part of a *C. elegans.*
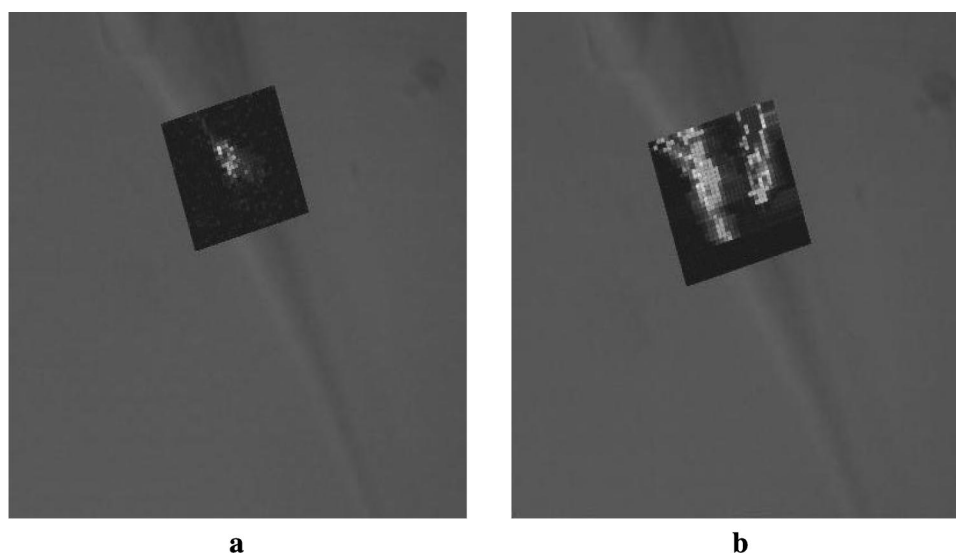
Fig. 4 Two-photon excitation fluorescence image (a) and second-harmonic generation image (b) respectively. Images were obtained from the posterior part of a *C. elegans*.

this region. Moreover, the structures of high SHG intensity on the body edges of the worm [Fig. 3(b)] appear to have a thickness of $2-3$ μm, which corresponds, to the real thickness of hypodermis of *C. elegans*. Consequently, collagen, which is one of the basic ingredients of the hypodermis, and actomyosin, seem to be the main components that contribute in the detection of the SHG signal from the outline of the nematode. In the strain we used in this experiment the GFP molecules are expressed under the control of the myo-2 promoter. This promoter is tissue specific and the GFP expression is limited to the cytoplasm of the pharyngeal muscle cells. Therefore, the GFP molecules, due to their random orientation in the pharynx region do not contribute to the SHG signal. It is worth mentioning that the obtained SHG images are similar with images from other very recent studies.[15] In our work the use of 1028 nm as the excitation source, instead of a typical wavelength around the 800 nm, was chosen in order to reduce more of the photodamage effects onto the specimens, due to the lower power per photon.

By using TPEF imaging we were able to detect the inner part of the pharynx due to excitation of the GFP molecules in pharyngeal muscles. Additionally, it is feasible to image the pharynx and the outline of the worm by performing SHG measurements. Thus the two images [TPEF Fig. 3(a), SHG Fig. 3(b)] provide complementary information about the biological sample. This is due to the fact that the induced signals come from different components. The endogenous structural proteins, especially actomyosin complexes and collagen, are responsible for the observation of SHG signals. On the other hand, the diffused GFP molecules are the main contributors for the detection of TPEF signals.

We investigated the feasibility of detecting different cell types of *C. elegans* by performing similar measurements with two out of the six touch receptor neurons in the posterior end of the worm. In these experiments, GFP was expressed under the mec-4 touch-cell specific promoter at high levels and was localized in the cytoplasm of these neurons. Such high GFP levels result in significantly enhanced recorded TPEF signals,

since the detection was performed in a spectral region with bandwidth of 1 nm. Figure 4(a) depicts a TPEF image from the posterior part of a sample. The signal was recorded from below. The monochromator was tuned at 525 nm. The dimensions of the scanning region were 30×30 μm^2. The scanning was performed in a specific z position where the TPEF signal emanates from one neuron was maximum. The recorded signal comes from the cytoplasmic GFP molecules, which are expressed in the six neuronal cells of the worm. It is obvious from the collected image [Fig. 4(a)] that in a specific z position, it is possible to detect the precise localization of one of the two touch receptor neurons which are lying near the tail of the *C. elegans*.

Figure 4(b) presents the same scanning of the sample but in this case the monochromator was tuned at 514 nm (SHG measurements). It is expected that in the posterior part of the *C. elegans* the muscle abundance is limited. However, as is shown in Fig. 4(b), the SHG enabled us to detect the contour of the tail. The endogenous structural proteins, especially the collagen, are the main contributors to the recorded SHG signals. The GFP molecules in the neuronal cell are symmetrically distributed, so the contribution to the observed signal of SHG can be excluded. This is in good agreement with the experimental data, since it was not feasible to detect the neuronal cell, as depicted in Fig. 4(b). The same kind of measurements (at 514 nm) was performed at various z positions. In all of these images, it was impossible to locate the neurons (images are not presented). From the above mentioned observations, it is once again clear that the two types of images (SHG versus TPEF) could provide complementary information. By obtaining TPEF images in a specific z position we are able to localize one of the two mechanoreceptor neuronal cells which are lying in the posterior part of the worm due to the contribution of GFP molecules to the collected signal. By performing the same SHG imaging we obtain information concerning the cuticle, the contour, and the muscles of the worm due to the contribution of the structural protein arrays to the recorded signal.

5 Conclusions

The combination of SHG and TPEF high-resolution imaging is a new, very promising technique which is expected to be a useful and unique tool in various fields of medicine and biology, since it can provide a detailed picture of tissue (especially the SHG imaging). However, the main inhibitory reason for the extended application of this innovative technique to the biological community is that the commercial two-photon microscopes are very expensive. In the present study a compact, reliable, flexible, inexpensive (except for the laser component) experimental apparatus has been developed. A properly modified, common, inexpensive microscope was employed. A low-cost motorized *xyz* translation stage was used for the scanning procedure. The time interval for the realization of the *in vivo* measurements in *C. elegans* was more than two hours during our experiments. Consequently, stage scanning was appropriate for obtaining a sufficient number of detailed *in vivo* images of the specific biological specimens. Moreover, this inexpensive experimental setup is preferable for single point measurements onto the neurons of the worm, in order to monitor the membrane potential via alterations in SHG signals. These measurements that comprise our potential main future target could provide valuable and unique information for the transduction of mechanical signals in the mechanotranducer neuronal cells of *C. elegans*. Thus, we developed a system that can be easily used for a variety of experiments in the field of biology.

By using this system, it is feasible to collect both SHG and TPEF signals in distinct sets of measurements or simultaneously by detecting SHG images from below and TPEF images from above. We obtained detailed images of the *C. elegans* body by recording nonlinear phenomena at the microscopic level. Reliable and valuable information in real time concerning the structure and the morphology of the *C. elegans* were obtained by using this inexpensive prototype system.

References

1. W. Denk, J. H. Strickler, and W. W. Webb, "Two-photon laser scanning fluorescence microscopy," *Science* **248**, 73 (1990).
2. S. Maiti, R. M. Williams, J. B. Shear, W. R. Zipfel, and W. W. Webb, "Measuring serotonin distribution in live cells with three-photon excitation," *Science* **24**, 530–532 (1997).
3. C. Xu, W. Zipfel, J. B. Shear, R. M. Williams, and W. W. Webb, "Multiphoton fluorescence excitation: new spectral windows for biological nonlinear microscopy," *Proc. Natl. Acad. Sci. U.S.A.* **93**, 10763–10768 (1996).
4. L. Moreaux, O. Sandre, M. Blanchard-Desce, and J. Mertz, "Membrane imaging by simultaneous second-harmonic and two-photon microscopy," *Opt. Lett.* **25**, 320–322 (2000).
5. W. Mohler, A. C. Millard, and P. J. Campagnola, "Second harmonic generation imaging of endogenous structural proteins," *Methods* **29**, 97–109 (2003).
6. N. Bloembergen, *Nonlinear Optics*, World Scientific, Singapore (1965).
7. G. Cox and C. J. R. Sheppard, "Practical limits of resolution in confocal and non-linear microscopy," *Microsc. Res. Tech.* **63**, 18–22 (2004).
8. T. F. Heinz, C. K. Chen, D. Richard, and Y. R. Shen, "Spectroscopy of molecular monolayers by resonant second-harmonic generation," *Phys. Rev. Lett.* **48**, 478–481 (1982).
9. L. Moreaux, O. Sandre, and J. Mertz, "Membrane imaging by second-harmonic generation microscopy," *J. Opt. Soc. Am. B* **17**, 1685–1694 (2000).
10. J. Mertz and L. Moreaux, "Second-harmonic generation by focused excitation of inhomogeneously distributed scatterers," *Opt. Commun.* **196**, 325–330 (2001).
11. A. T. Yeh, N. Nassif, A. Zoumi, and B. J. Tromberg, "Selective corneal imaging combined second-harmonic generation and two-photon excited fluorescence," *Opt. Lett.* **27**, 2082–2084 (2002).
12. A. Zoumi, A. Yeh, and B. J. Tromberg, "Imaging cells and extracellular matrix in vivo by using second-harmonic generation and two-photon excited fluorescence," *Proc. Natl. Acad. Sci. U.S.A.* **99**, 11014–11019 (2002).
13. E. Brown, T. McKee, E. diTomaso, A. Pluen, B. Seed, Y. Boucher, and R. K. Jain, "Dynamic imaging of collagen and its modulation in tumors in vivo using second-harmonic generation," *Nat. Med.* **9**, 796–800 (2003).
14. L. Moreaux, O. Sandre, S. Charpak, M. Blanchard-Desce, and J. Mertz, "Coherent scattering in multi-harmonic light microscopy," *Biophys. J.* **80**, 1568–1574 (2001).
15. P. J. Campagnola and L. M. Loew, "Second-harmonic imaging microscopy for visualizing biomolecular arrays in cells, tissues and organisms," *Nat. Biotechnol.* **21**, 1356–1360 (2003).
16. D. A. Kleinman, "Nonlinear dielectric polarization in optical media," *Phys. Rev.* **126**, 1977–1979 (1962).
17. R. Hellwarth and P. Christensen, "Nonlinear optical microscopic examination of structure in polycrystalline ZnSe," *Opt. Commun.* **12**, 318–322 (1974).
18. I. Freund, M. Deutsch, and A. Sprecher, "Connective tissue polarity," *Biophys. J.* **50**, 693–712 (1986).
19. P. J. Campagnola, A. C. Millard, M. Terasaki, P. E. Hoppe, C. J. Malone, and W. A. Mohler, "Three-dimensional high-resolution second-harmonic generation imaging of endogenous structural proteins in biological tissues," *Biophys. J.* **81**, 493–508 (2002).
20. P. Stoller, P. M. Celliers, K. M. Reiser, and A. M. Rubenchik, "Quantitative second-harmonic generation microscopy in collagen," *Appl. Opt.* **42**, 5209–5219 (2003).
21. G. Cox, E. Kable, A. Jones, I. Fraser, F. Manconi, and M. D. Gorrell, "3-dimensional imaging of collagen using second harmonic generation," *J. Struct. Biol.* **141**, 53–62 (2003).
22. Y. Guo, P. P. Ho, H. Savage, D. Harris, P. Sacks, S. Schantz, F. Liu, N. Zhadin, and R. R. Alfano, "Second-harmonic tomography of tissues," *Opt. Lett.* **22**, 1323–1325 (1997).
23. E. Brown, T. McKee, E. di Tomaso, A. Pluen, B. Seed, Y. Boucher, and R. K. Jain, "Dynamic imaging of collagen and its modulation in tumors in vivo using second-harmonic generation," *Nat. Med.* **9**, 796–801 (2003).
24. S. Roth and I. Freund, "Second-harmonic generation in collagen," *J. Chem. Phys.* **70**, 1637–1643 (1979).
25. P. J. Campagnola, H. A. Clark, W. A. Mohler, A. Lewis, and L. M. Loew, "Second-harmonic imaging microscopy of living cells," *J. Biomed. Opt.* **6**, 277–286 (2001).
26. S. Roth and I. Freund, "Optical second-harmonic scattering in rat-tail tendon," *Biopolymers* **20**, 1271–1290 (1981).
27. E. Georgiou, T. Theodossiou, V. Hovhannisva, K. Politopoulos, G. S. Rapti, and D. Yova, "Second and third optical harmonic generation in type I collagen, by nanosecond laser irradiation, over a broad spectral region," *Opt. Commun.* **176**, 253–260 (2000).
28. O. Bouevitch, A. Lewis, I. Pinevsky, J. P. Wuskell, and L. M. Loew, "Probing membrane potential with nonlinear optics," *Biophys. J.* **65**, 672–679 (1993).
29. I. Ben-Oren, G. Peleg, A. Lewis, B. Minke, and L. Loew, "Infrared nonlinear optical measurements of membrane potential in photoreceptor cells," *Biophys. J.* **71**, 1616–1620 (1996).
30. G. Peleg, A. Lewis, M. Linial, and L. M. Loew, "Nonlinear optical measurement of membrane potential around single molecules at se-

lected cellular sites,'' *Proc. Natl. Acad. Sci. U.S.A.* **96**, 6700–6704 (1999).

31. P. J. Campagnola, M. de Wei, A. Lewis, and L. M. Loew, ''High-resolution nonlinear optical imaging of live cells by second harmonic generation,'' *Biophys. J.* **77**, 3341–3349 (1999).

32. A. Lewis, A. Khatchatouriants, M. Treinin, M. Sheves, G. Peleg, Z. Chen, O. Bouevitch, Z. Rothman, and L. Loew, ''Second harmonic generation of biological interfaces: probing membrane proteins and imaging membrane potential around single molecules,'' *Chem. Phys.* **245**, 133–143 (1999).

33. L. Moreaux, T. Pons, V. Dambrin, M. Blanchard-Desce, and J. Mertz, ''Electro-optic response of second-harmonic generation membrane potential sensors,'' *Opt. Lett.* **28**, 625–627 (2003).

34. A. C. Millard, L. Jin, A. Lewis, and L. M. Loew, ''Direct measurement of the voltage sensitivity of second-harmonic generation from a membrane dye in patch-clamped cells,'' *Opt. Lett.* **28**, 1221–1223 (2003).

35. T. Pons, L. Moreaux, O. Mongin, M. Blanchard-Desce, and J. Mertz, ''Mechanisms of membrane potential sensing with second-harmonic generation microscopy,'' *J. Biomed. Opt.* **8**, 428–431 (2003).

36. J. Y. Huang, Z. Chen, and A. Lewis, ''Second harmonic generation in purple membrane-poly(vinyl alcohol) films: probing the dipolar characteristics of the bacteriorhodopsin chromophore in bR570 and M412,'' *J. Phys. C* **93**, 3314–3323 (1989).

37. A. Khatchatouriants, A. Lewis, Z. Rothman, L. Loew, and M. Treinin, ''GFP is a selective non-linear optical sensor of electrophysiological processes in *Caenorhabditis elegans*,'' *Biophys. J.* **79**, 2345–2352 (2000).

38. J. E. Sulston, E. Schierenberg, J. G. White, and J. N. Thomson, ''The embryonic cell lineage of the nematode *Caenorhabditis elegans*,'' *Dev. Biol.* **100**, 64–119 (1983).

39. The *C. elegans* Sequencing Consortium, ''Genome sequence of the nematode C. elegans: a platform for investigating biology,'' *Science* **282**, 2012–2018 (1998).

40. A. Fire, S. Xu, M. K. Montgomery, S. A. Kostas, S. E. Driver, and C. Mello, ''Potent and specific genetic interference by double-stranded RNA in *Caenorhabditis elegans*,'' *Nature (London)* **391**, 806–811 (1998).

41. C. C. Mello, J. M. Kramer, D. Stinchcomb, and V. Ambros, ''Efficient gene transfer in *C. elegans*: extrachromosomal maintenance and integration of transforming sequences,'' *EMBO J.* **10**, 3959–3970 (1991).

42. J. G. White, E. Southgate, J. N. Thomson, and S. Brenner, ''The structure of the nervous system of *Caenorhabditis elegans*,'' *Proc. R. Soc. London, Ser. B* **314**, 1–340 (1996).

43. C. I. Bargmann, ''Neurobiology of the *Caenorhabditis elegans* genome,'' *Science* **282**, 2028–2033 (1998).

44. C. I. Bargmann and J. M. Kaplan, ''Signal transduction in the *Caenorhabditis elegans* nervous system,'' *Annu. Rev. Neurosci.* **21**, 279–308 (1998).

45. C. H. Rankin, ''From gene to identified neuron to behaviour in *Caenorhabditis elegans*,'' *Nat. Rev. Genet.* **3**, 622–630 (2002).

46. S. Brenner, ''The genetics of *Caenorhabditis elegans*,'' *Genetics* **77**, 71–94 (1974).